Supplementary Material to OP3 CCN-HTDMA Reconciliation Study

Section 1.1 shows the sigmoid function used to derive both critical supersaturation ($S_{c,D0}$) and the dry diameter at which 50% of the particles have activated ($D_{50,S}$) are calculated from CCNc and CPC data, as described in the main text.
Section 1.2 highlights the specific CCNc measurement uncertainties and their calculation and Section 1.3 shows how the standard errors associated with the HTDMA measurements were calculated.

1 Definition of terms and calculation procedures

1.1 Fitting S-step and D-step CCNc data

Defined in the main text, the fitting function used for deriving the point at which $F_A(S, D_0) = 0.5$ is a sigmoidal function using orthogonal distance regression (ODR), weighted according to the associated errors in each axis, using the Igor Pro software package and associated libraries (*ODRPACK95*, Boggs et al. 1989).

$$y = K_0 + \frac{K_1}{1 + \exp\left((x - K_2)/K_3\right)} \tag{S1}$$

Where K_0 is the base of the sigmoid (held to zero), K_1 is the maximum on the sigmoid (unconstrained to to minimise effects caused by systematic inaccuracies of either instrument), K_2 is the x value at which $y = 0.5$ (either, $D_{50,S}$ or $S_{c,D0}$, depending on the x-axis used) and K_3 is the rate.

This function is used to derive both $D_{50,S}$ and $S_{c,D0}$ for CCNc data. The fitting algorithm outputs a standard error of the x-axis value at $y = 0.5$, shown in Figures S2 and S3. These errors are propagated through to further calculations of quantities such as D_{thres} and N_{CCN}. The standard error from S-step analysis is larger as the data consists of only 5 data points (each S_{set}) and hence is more sensitive to the relative positions of these data. Fitting D-step interpreted data results in a smaller standard error, Figures S2 and S3, as there are many more data points and thus higher resolution around each $D_{50,S}$.

1.2 CCNc Measurement Uncertainty

1.2.1 Uncertainty in S_{set}

In order to estimate the uncertainty in S from the standard deviation of these quantities, the standard deviation (σ) of each measurement of temperature, flow and pressure (T, Q and P respectively, which are taken to vary independently) is multiplied by its differential value, summed in quadrature and divided by the square root of the number of observations (N; number of particles measured during an averaging period) to give the standard error in S:

$$\Delta S = \frac{\sqrt{\left(\frac{\partial S}{\partial T}\sigma T\right)^2 + \left(\frac{\partial S}{\partial Q}\sigma Q\right)^2 + \left(\frac{\partial S}{\partial P}\sigma P\right)^2}}{\sqrt{N}} \tag{S2}$$

The dependence of ΔS on $\sqrt{N}$ arises because the instrument detector (the OPC) only samples the conditions when a particle is detected. As T, Q and P have been assumed to vary randomly throughout the measurement period, the more particles detected, the more precise the average supersaturation will be.

1.2.2 Uncertainty in D_0

The range of diameters introduced into the CCNc for a given target diameter is described by the DMA transfer function. For this analysis, we have assumed an ideal, triangular transfer function (Knutson and Whitby, 1975), with symmetrical bounds 5% either side of the target dry diameter, D_T. One standard deviation of this transfer function is described by $\sigma = c\sqrt{1/6}$, where $c = 0.1D_T$ i.e. the width of the base of the transfer function. When propagating the error associated with the diameter measurement of D_T, the standard error of D_T has been used:

$$\Delta D_T = \frac{c\sqrt{(1/6)}}{\sqrt{N}} \tag{S3}$$

where N is the number of particles counted.

1.2.3 Uncertainty in number concentration

The CCNc and CPC number concentration standard errors have been calculated by invoking Poisson statistics:

$$\Delta(\sum N) = \sqrt{\frac{\sum N}{Q \sum T}} \tag{S4}$$

where N is the number of particles counted, substituted by either CCNc ($N(S, D_0)$) or CPC ($N(D_0)$), Q is the flow rate and T is the sampling time. The uncertainty in N is calculated and then propagated through the multiple charging correction procedure.

The error associated with the activated fraction, $F_A(S, D_0)$ can then be calculated:

$$\Delta(\sum F_A(S, D_0)) = \frac{N(S, D_0)}{N(D_0)} \sqrt{\left(\frac{\Delta(\sum N(S, D_0))}{N(S, D_0)}\right)^2 + \left(\frac{\Delta(\sum N(D_0))}{N(D_0)}\right)^2} \tag{S5}$$

1.3 HTDMA errors

The hygroscopic growth factor probability distribution $p(GF)$ was corrected for small deviations (typically ±2%RH) from the setpoint RH, as outlined by Gysel et al. (2009) and calculated as follows:

$$\overline{GF}_{D_0,RH,c} = \left(1 + (\overline{GF}^3_{D_0,RH_m} - 1)\frac{(1-RH_m)RH_t}{(1-RH_t)RH_m}\right)^{\frac{1}{3}} \quad \text{(S6)}$$

where $\overline{GF}_{D_0,RH,c}$ is the RH-corrected, mean, hyrgoscopic growth factor for a particle of dry diameter D_0, $\overline{GF}_{D_0,RH_m}$ is the uncorrected mean growth factor, RH_m is the measured RH and RH_t is the target RH. A full explanation of the correction applied is described by Gysel et al. (2009).

In order to propagate the error associated with the change in growth factor from this correction, Eq. S6 is differentiated with respect to RH_m to give:

$$\frac{\partial(\overline{GF}_{D_0,RH,c})}{\partial(RH_m)} = -\left((\overline{GF}_{D_0,RH_m} - 1)\frac{RH_t}{(1-RH_t)}\frac{1}{(RH_m)^2}\right)^{-\frac{1}{3}} \quad \text{(S7)}$$

An error simulation which forms part of the TDMAinv analysis was used on the data, with the results from the error simulation showing the sensitivity of the inversion result to small changes in the measurement due to added noise (incorporating counting statistics). This helps in, for example, judging whether two peaks in the growth factor probability distribution function, $p(GF)$, can be attributed to distinct modes or whether the structure of the $p(GF)$ can be reliably attributed to distinct modes or whether they are indistinguishable from instrument noise. This is outlined in detail by Gysel et al. (2009) and is shown in Figs. 4B and C therein. 100 error simulations are performed on $p(GF)$ for each growth factor bin, and the statistical mean of these taken. The standard deviation of the mean 100 simulations was then calculated, representing the effects of counting statistics and variability in size measurement, denoted by $\sigma_{p(GF)}$. These two errors are summed in quadrature, representing the HTDMA error, GF_{error}:

$$GF_{error} = \sqrt{\left(\frac{\partial(\overline{GF}_{D_0,RH,c})}{\partial(RH_m)}0.015\right)^2 + {\sigma_{p(GF)}}^2} \quad \text{(S8)}$$

where 0.015 relates to the precision of the measurement of RH (1.5%) within the HTDMA used for the COPS experiment.

References

[Boggs et al. (1989)] Boggs, P., Donaldson, J., Byrd, R., and Schnabel, R.: Algorithm 676: ODRPACK: software for weighted orthogonal distance regression, ACM Transactions on Mathematical Software (TOMS), 15, 364, 1989.

[Gysel et al. (2009)] Gysel, M., McFiggans, G., and Coe, H.: Inversion of tandem differential mobility analyser (TDMA) measurements, Journal of aerosol science, 40, 134–151, 2009.

[Knutson and Whitby (1975)] Knutson, E. and Whitby, K.: Aerosol classification by electric mobility: apparatus, theory, and applications, Journal of Aerosol Science, 6, 443–451, 1975.

[Rose et al. (2008)] Rose, D., Gunthe, S., Mikhailov, E., Frank, G., and Dusek, U.: Calibration and measurement uncertainties of a continuous-flow cloud condensation nuclei counter (DMT-CCNC): CCN activation of ammonium sulphate and sodium chloride particles in theory and experiment, Atmos. Chem. Phys, 8, 1153–1179, 2008.

2 Supplementary figures

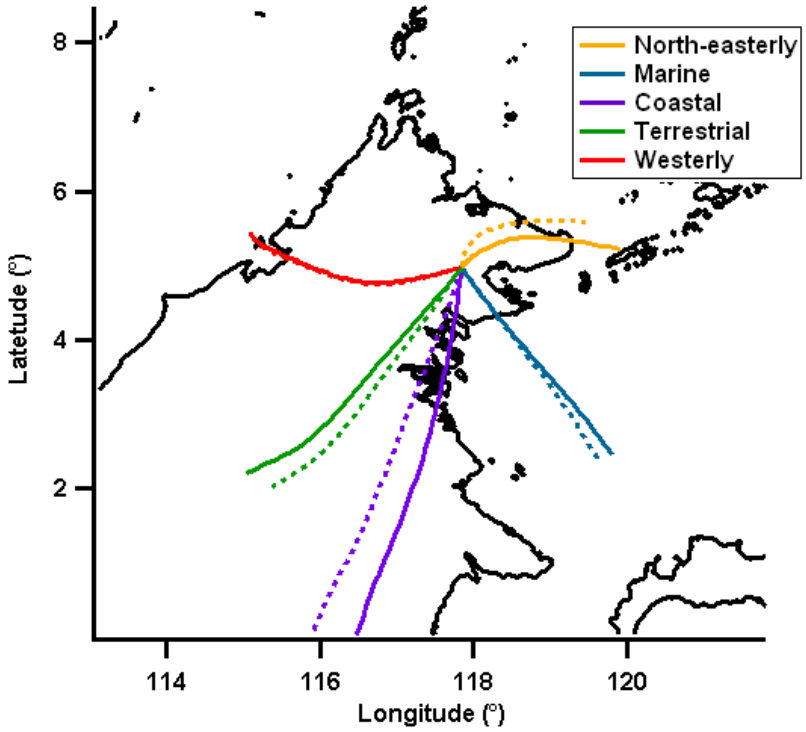

Figure S1: This plot shows the period classification mean latitude and longitude. The solid and dashed lines represent alternate back trajectory calculations. The majority of the data presented from OP3-III was attributed to Marine and Terrestrial clusters.

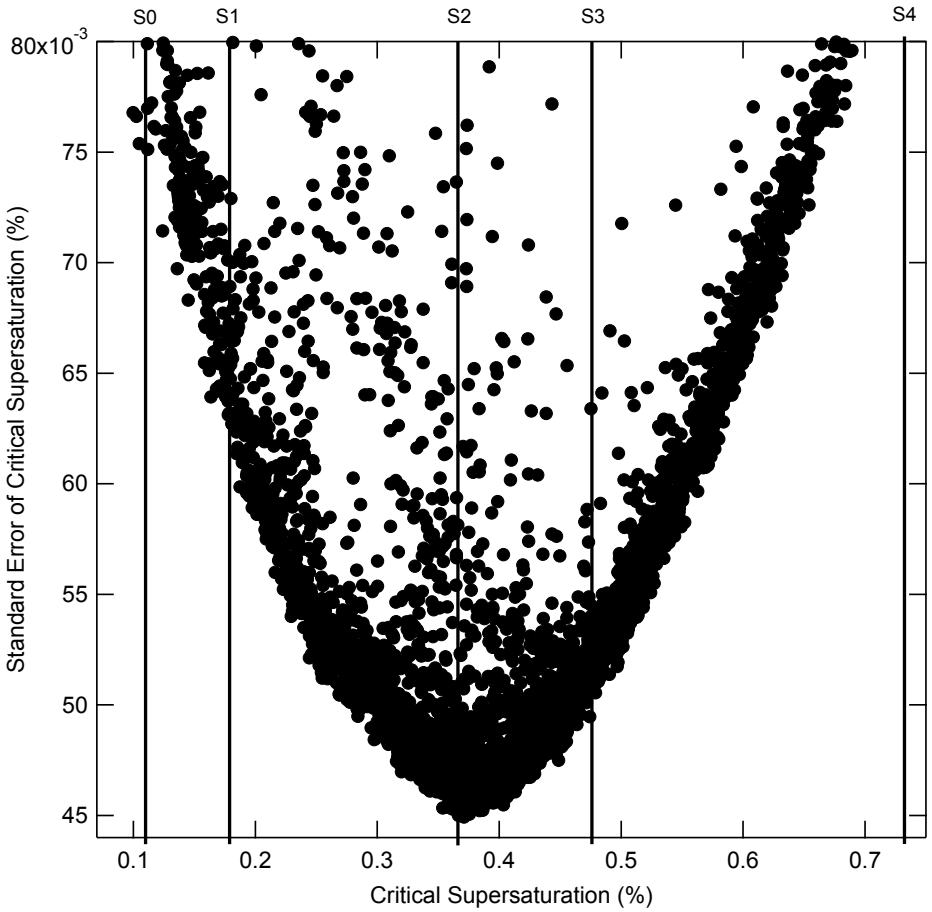

Figure S2: This plot shows the standard error of $S_{c,D0}$ plotted against the derivation of $S_{c,D0}$ from S-step analysis. The derivation of $S_{c,D0}$ has the smallest error at the central S_{set} (S2). The closer the derived $S_{c,D0}$ of the particle to that of the bounds of the measurement (S0; S4), the larger the error from the fitting of the sigmoid. Data with large (relative) errors but a $S_{c,D0}$ between S1 and S3 may be influenced by mixing state or other variables within the sigmoid fitting function.

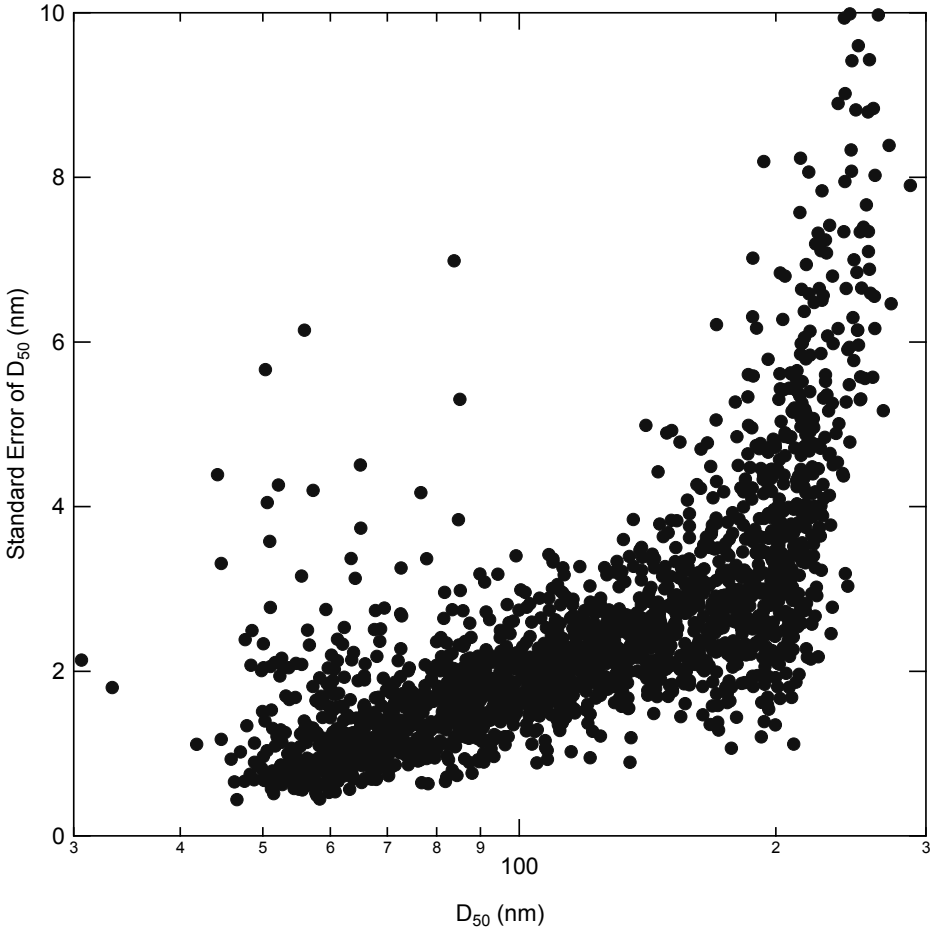

Figure S3: The error associated with fitting data using D-step analysis is, as expected, different to that associated with S-step analysed data. Only at over 200 nm does the error increase significantly. This is because, as shown in Figure 2, the fraction of aerosol activated (on average) is over 50% at the lowest supersaturation. When F_A is just under 50% then the error will be large, but if over 50% then no sigmoid can be plotted.

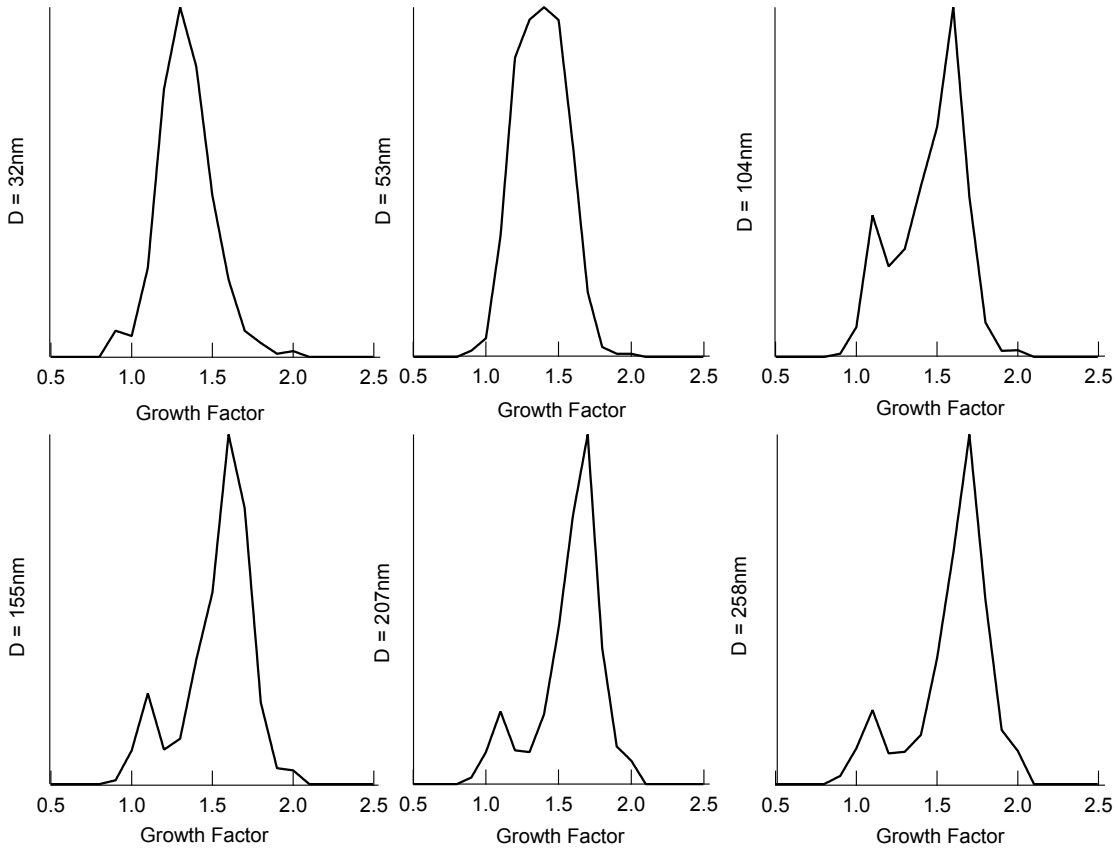

Figure S4: A graph showing the average of each growth factor bin of $p(GF)$, for each dry diameter as measured by the HTDMA. The degree of external mixing increases with size above 53 nm, below which the aerosol appears to be internally mixed or contain a narrow range of external mixtures.

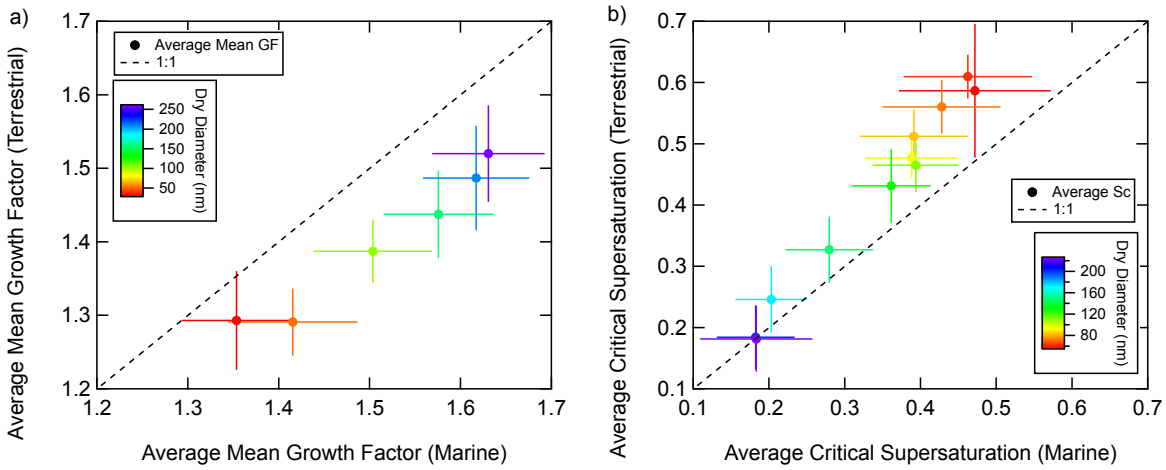

Figure S5: a) The RH corrected mean growth factor and b) critical supersaturation for terrestrial sectors plotted against marine sectors, as a function of dry particle diameter - indicated by the colourscale. The error bars denote the standard deviation.

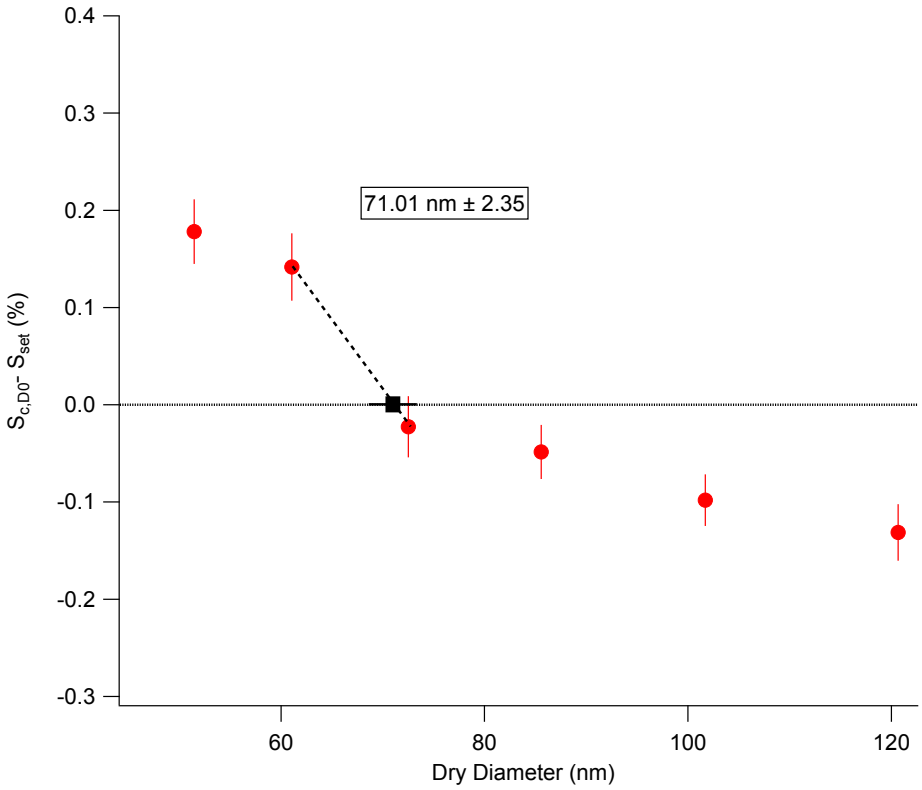

Figure S6: A graph showing $S_{c,D_0} - S_{set}$ vs D_0. The two data points straddling the zero line are linearly interpolated between, with the intercept defining the physical threshold diameter of the aerosol, $D_{thres,Sc}$. The errors on $D_{thres,Sc}$ are propagated using standard procedure.

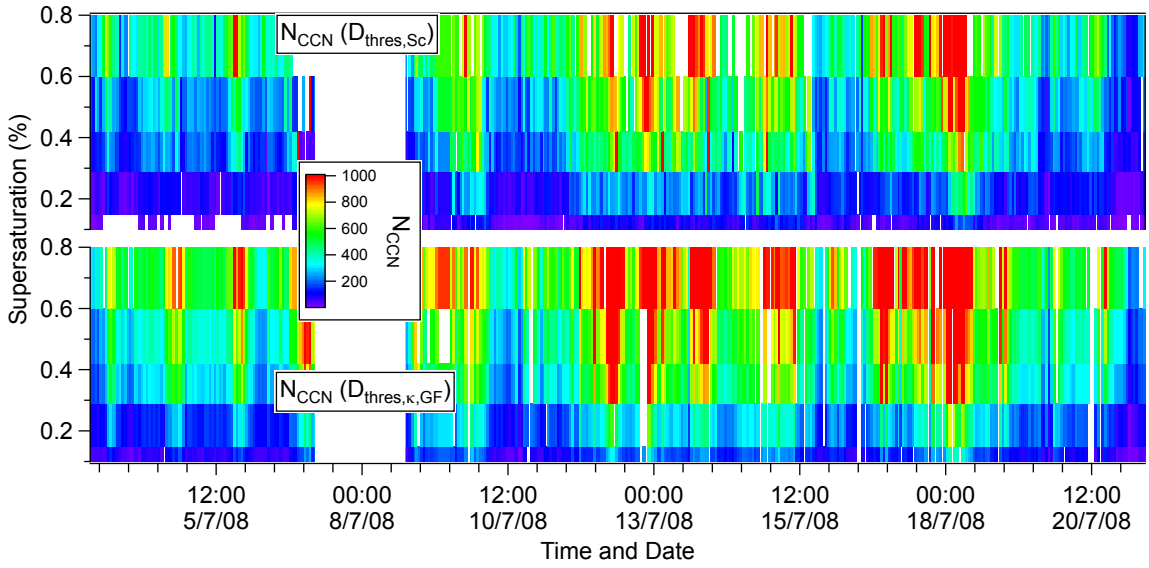

Figure S7: A time series for the OP3-III campaign showing a comparison of predicted N_{CCN} from CCNc (top) S-step analysis and HTDMA measurements respectively, as a function of bin-edge supersaturation (left axis).